# Article

**Cell** PRESS

# Intravital Imaging Reveals Limited Antigen Presentation and T Cell Effector Function in Mycobacterial Granulomas

Jackson G. Egen,[1,5,6] Antonio Gigliotti Rothfuchs,[2,5,7] Carl G. Feng,[2] Marcus A. Horwitz,[4] Alan Sher,[2] and Ronald N. Germain[1,3,*]

[1]Lymphocyte Biology Section, Laboratory of Immunology
[2]Immunobiology Section, Laboratory of Parasitic Diseases
[3]Program in Systems Immunology and Infectious Disease Modeling
National Institute of Allergy and Infectious Diseases, National Institutes of Health, Bethesda, MD 20892, USA
[4]Division of Infectious Diseases, Department of Medicine, University of California-Los Angeles School of Medicine, Los Angeles, CA 90095, USA
[5]These authors contributed equally to this work
[6]Present address: Genentech, 1 DNA Way, MS34, South San Francisco, CA 94080, USA
[7]Present address: Department of Microbiology, Tumor and Cell Biology, Karolinska Institutet, Nobels väg 16, 171 77 Stockholm, Sweden
*Correspondence: rgermain@nih.gov
DOI 10.1016/j.immuni.2011.03.022

## SUMMARY

**Cell-mediated adaptive immunity is critical for host defense, but little is known about T cell behavior during delivery of effector function. Here we investigate relationships among antigen presentation, T cell motility, and local production of effector cytokines by CD4+ T cells within hepatic granulomas triggered by Bacille Calmette-Guérin or *Mycobacterium tuberculosis*. At steady-state, only small fractions of mycobacteria-specific T cells showed antigen-induced migration arrest within granulomas, resulting in low-level, polarized secretion of cytokines. However, exogenous antigen elicited rapid arrest and robust cytokine production by the vast majority of effector T cells. These findings suggest that limited antigen presentation and/or recognition within granulomas evoke a muted T cell response drawing on only a fraction of the host's potential effector capacity. Our results provide new insights into the regulation of host-protective functions, especially how antigen availability influences T cell dynamics and, in turn, effector T cell function during chronic infection.**

## INTRODUCTION

During the typical adaptive immune response to an infectious agent, T cell interactions with cognate antigen-bearing dendritic cells (DCs) in secondary lymphoid organs induce a program of proliferation and differentiation resulting in production of an effector T cell population with the capacity to home to sites of inflammation and produce factors critical for containment and/or clearance of the infection. This targeted delivery of effector function is dependent on antigen-specific interactions with antigen-presenting cells (APCs) within the infected tissue. Elucidating the relationship between effector T cell-APC interactions at sites of infection and the subsequent expression of effector molecules by T cells is critical for deciphering the basis of productive and nonproductive adaptive immune responses and for advancing our capacity to develop new vaccines that rely on such cell-mediated responses.

T cell-mediated immunity plays a major role in host defense against intracellular microbial pathogens. Infection with *Mycobacterium* species such as *M. tuberculosis* (Mtb) induces formation of granulomas, agglomerations of inflammatory myeloid cells and effector lymphocytes considered crucial for control of mycobacterial replication, and maintenance of the infection in an asymptomatic state. Past studies have examined the static, spatial distribution of cells within these lesions, providing insight into the role(s) played by intragranuloma cell populations in effective resistance to bacterial growth and dissemination (Saunders and Britton, 2007; Ulrichs and Kaufmann, 2006). Clearly, αβ T cell receptor (TCR)+CD4+ T cells are critical for generating protective responses against mycobacterial infections (Caruso et al., 1999; Ladel et al., 1995; Mogues et al., 2001), at least in part based on their ability to locally produce inflammatory cytokines such as IFN-γ and TNF-α that enhance antimicrobial capacities of infected macrophages (Flynn and Chan, 2001). However, the dynamics of effector T cells migrating through and within granulomas, the frequency with which these lymphocytes are activated to full effector functionality, and the precise location of effector molecule delivery are all largely unstudied features of this critical adaptive immune response.

Until recently, the tools necessary to address these questions have been limited. However, advanced dynamic imaging methods now permit extending the knowledge gained from ex vivo or indirect in vivo studies to direct observation of immune cell behavior and function within complex tissues. One major application of such intravital microscopy (IM) techniques has been the analysis of naive T cell motility during antigen-specific activation by DCs in lymph nodes (LNs) (Bousso and Robey, 2003; Mempel et al., 2004; Miller et al., 2002, 2004; Stoll et al., 2002). Among other findings, these studies characterized the

altered migration patterns, decreased velocity, and in many cases, frank migration arrest resulting from antigen-specific T cell-APC interactions, thereby establishing the utility of IM for probing antigen presentation in situ (Bousso, 2008). More recently, imaging studies involving infection of the liver, brain, and skin with various pathogens or during autoimmune processes have begun to address the sequence of interactions between APCs and antigen-specific effector T cell subsets in nonlymphoid sites (Bartholomäus et al., 2009; Beattie et al., 2010; Fife et al., 2009; Filipe-Santos et al., 2009; Kawakami et al., 2005; Kim et al., 2009; Matheu et al., 2008; Schaeffer et al., 2009; Wilson et al., 2009). The findings of these recent analyses are generally in agreement with the phenomenon first observed during T cell priming in LNs, namely that T cells display a constrained migratory pattern and/or arrest on APCs upon antigen encounter, although the alterations in effector T cell motility in inflamed sites are reportedly more subtle and heterogeneous than during naive T cell activation in lymphoid tissues.

Although these efforts have partially characterized the dynamic behavior of effector T cells at sites of chronic infection, there remains a paucity of information regarding the coupling of T cell motility with the execution of effector function. Importantly, issues such as the fraction of effectors that are actively producing cytokines, the amount of cytokine production by such antigen-triggered cells, the polarity or lack thereof in the secretion of the effector molecules, and the kinetic relationship between changes in cell dynamics instigated by peripheral antigen recognition and the production of effector molecules are all critical aspects of the adaptive T cell response in tissues that are largely unexplored.

To begin to address these issues, we utilized multiphoton IM and flow cytometry to explore the process of antigen recognition by mycobacteria-specific CD4$^+$ T cells within hepatic granulomas. We showed that initial recruitment into and short-term retention of T cells within granulomas was independent of antigen recognition. Unexpectedly, antigen-specific and nonspecific T cell populations displayed only minor differences in motility after recruitment into granulomas, a finding that correlated with an extremely low frequency of mycobacteria-specific T cells actively producing low amounts of IFN-$\gamma$ and/or TNF-$\alpha$ within these lesions. These data suggest that for the vast majority of antigen-specific CD4$^+$ T cells migrating within a mycobacterial granuloma, local antigen presentation levels are insufficient to induce migrational arrest followed by polarized cytokine secretion. Our findings provide new insight into the substantial difference between ex vivo studies of T cell cytokine production by using maximal TCR stimulation and the actual amounts of cytokine elicited in response to physiological amounts of antigen presentation and point to the value of an increasing emphasis on a quantitative assessment of effector function in vivo to develop a better understanding of the pathways regulating host defense.

## RESULTS

### Antigen-Independent Recruitment Followed by Antigen-Dependent Activation of Effector T Cells

We previously demonstrated that activated, antigen nonspecific effector CD4$^+$ T cells are rapidly recruited into mycobacterial granulomas after adoptive transfer into infected animals (Egen et al., 2008). To examine the influence of antigen recognition on T cell behavior in this environment, we cotransferred differentially labeled, in vitro stimulated effector T cells derived from ovalbumin-specific OT-II TCR transgenic RAG1-deficient (OT-II) mice (Barnden et al., 1998) and mycobacterial antigen Ag85b-specific p25 TCR transgenic RAG1-deficient (p25) mice (Tamura et al., 2004) into animals infected 2 weeks earlier with an intravenous (i.v.) injection of 3 × 10$^6$ BCG or recombinant BCG-overexpressing Ag85b (rBCG30) (Horwitz et al., 2000). This latter strain was used to examine antigen-specific T cell responses under conditions of increased antigen expression. Animals were analyzed at 2 weeks postinfection (p.i.) based on evidence for substantial hepatic granuloma formation at this time point (Egen et al., 2008). Four hours after transfer, perfused livers were examined with immunofluorescence microcopy. As expected, both populations of effector T cells were efficiently recruited into hepatic granulomas (Figure 1A). However, no significant difference was observed in their initial recruitment and/or short-term retention (Figure 1B), suggesting that antigen does not play a primary role in regulating T cell trafficking into and out of granulomas over these time periods.

We next sought to determine whether mycobacteria-specific T cells were receiving TCR signals upon entering granulomas. In vitro stimulated OT-II and p25 T cells were cotransferred into previously infected hosts as above. Four hours after transfer, intrahepatic lymphocytes (IHLs) were analyzed by flow cytometry. This early time point was chosen based on our previous findings showing that in vitro stimulated T cells do not begin accumulating in large numbers within granulomas until 1–2 hr after transfer (Egen et al., 2008). Thus, we reasoned that 4 hr was sufficient for a bolus of effector T cells to enter a granuloma and receive TCR signals but not sufficient for hepatic T cells to have extensively trafficked within other infected tissues (e.g., spleen). As expected, OT-II T cells, whose cognate antigen ovalbumin was not present in these animals, showed no evidence of TCR-dependent activation after transfer into infected animals, as indicated by a lack of increased surface CD69 expression, arguing against antigen-independent upregulation of this surface protein under these conditions. In contrast, p25 T cells increased CD69 expression upon entry into infected livers, with the most profound increase observed in rBCG30-infected animals (Figures 1C and 1D). Thus, upon antigen-independent entry into granulomas, a substantial fraction of antigen-specific T cells engage antigenic complexes over relatively short periods of time. The finding that in comparison to BCG, rBCG30 infection induced higher CD69 expression by antigen-specific T cells also suggests that in BCG-induced granulomas, antigen presentation is not at saturating levels and can be driven higher by increasing antigen quantity.

### Limited Frequency of Sustained Antigen-Specific T Cell-APC Interactions within BCG-Induced Liver Granulomas

CD69 expression is typically induced in T cells by amounts of antigen or strengths of TCR signaling substantially below that necessary for cell division or cytokine production (Mempel et al., 2004; Sancho et al., 2005; Skokos et al., 2007). Previous studies have shown that T cells migrating through tissue parenchyma show reduced velocity upon antigen receptor
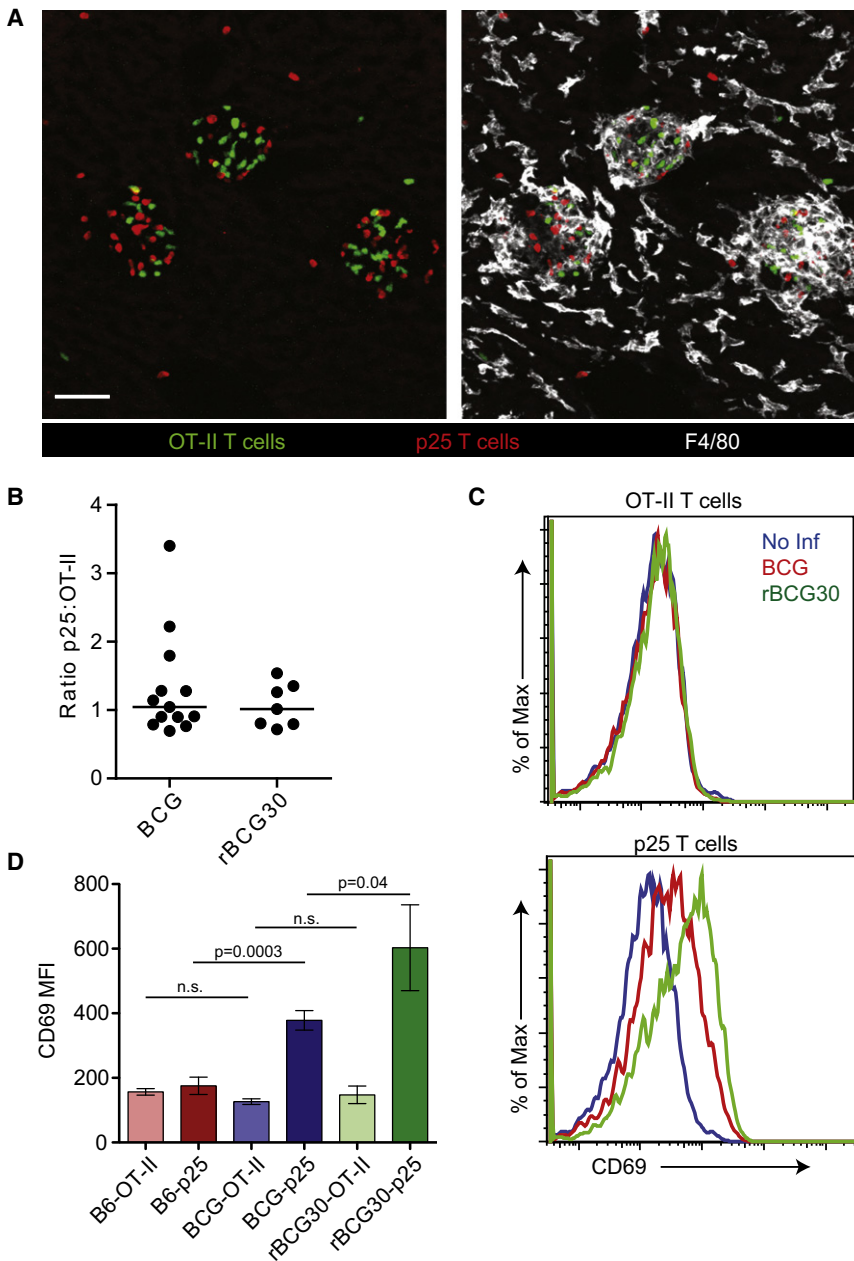
**Figure 1. Antigen-Independent Accumulation of T Cells in Mycobacterial Granulomas**

(A) CMFDA-labeled OT-II and CMTPX-labeled p25 in vitro-stimulated T cells were transferred i.v. into BCG-infected animals (2 weeks p.i.). Four hours later, livers were fixed, sectioned, and stained with an antibody specific for F4/80. Scale bar represents 50 μm.

(B) Numbers of transferred granuloma-associated T cells were quantified from at least ten images per mouse. Data points represent the ratio of p25 to OT-II T cells for individual mice compiled from at least three separate experiments.

(C) In vitro stimulated, dye-labeled T cells were transferred into infected mice as in (A). Four hours later, IHLs were purified from perfused livers, stained with CD4 and CD69, and analyzed by flow cytometry. Histograms show CD69 fluorescence of OT-II or p25 gated cells.

(D) Median fluorescence intensity (MFI) of CD69. Graph shows mean ± SD from three mice per group and is representative of three similar experiments. p values from a two-tailed t test are shown (n.s., not significant).
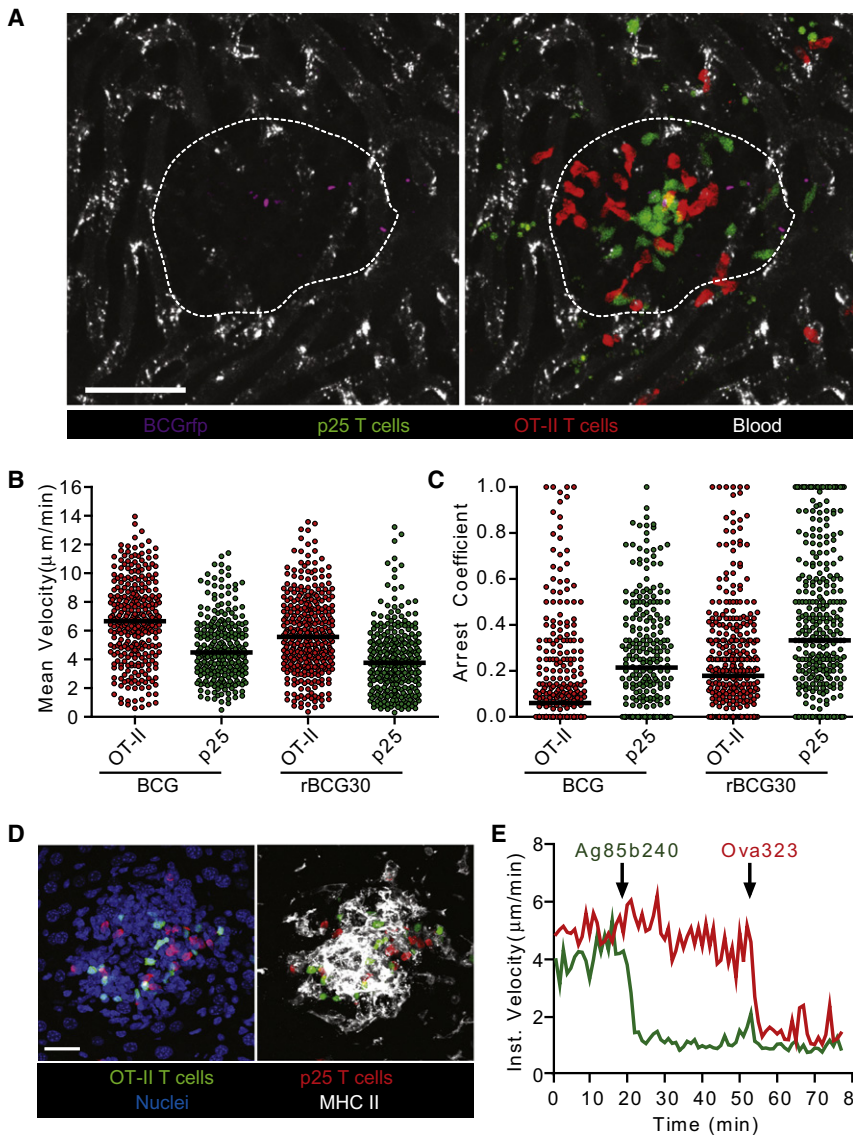
lomas contained a modest fraction of antigen-specific T cells displaying clear differences in motility compared to nonspecific control cells, other granulomas showed no obvious difference between these two T cell populations (Movie S1 available online). Importantly, all granulomas contained a predominant fraction of highly motile p25 T cells, suggesting that only a minor fraction of the mycobacteria-specific T cells received substantial TCR signals over these time periods. Quantitative cell tracking of OT-II and p25 T cells revealed subtle differences in mean velocity and arrest coefficient (which better reveals the fraction of cells undergoing antigen-induced stopping behavior) (Figures 2B and 2C). Consistent with their more pronounced upregulation of CD69, p25 T cells showed slightly greater reductions in motility in rBCG30-infected compared to BCG-infected animals. However, the motility of OT-II T cells also appeared slightly different between these two groups (Figures 2B and 2C), indicating that infection with these two agents may result in granuloma environments that differ by more than just antigen presentation levels.

To determine whether the above findings reflected low amounts of antigen presentation or were due to some other T cell-intrinsic or -extrinsic property that led to a dissociation of the expected correlation between migration behavior and strength of antigen recognition, we determined the maximal degree of T cell-migrational arrest that could be observed upon strong TCR engagement. Numerous APCs expressing high amounts of MHC class II surround granuloma-associated

engagement, with robust TCR stimulation under such conditions able to induce migration arrest (Bousso, 2008). Therefore, to probe for local high-level antigen presentation within granulomas, we used IM to examine the dynamic behavior of in vitro stimulated antigen-specific and nonspecific granuloma-associated effector T cells shortly after their adoptive transfer into previously infected animals. For some experiments, we utilized BCG expressing RFP (BCGrfp) (Abadie et al., 2005) to allow visualization of T cells in relation to individual mycobacteria present in the imaged granuloma (Figure 2A).

We found that the majority of OT-II and p25 T cells showed rapid migration that was constrained within the borders of the relevant granuloma over several hours. Whereas some granu-

**Figure 2. Antigen-Specific and Nonspecific T Cells Display Only Slight Differences in Motility within Mycobacterial Granulomas**

(A) CMFDA-labeled p25 and CMTPX-labeled OT-II T cells were transferred i.v. into mice that had been infected with BCGrfp (2 weeks p.i.). Four hours later, animals were injected i.v. with BSA-647 to label blood vessels and subjected to intravital hepatic imaging. Scale bar represents 50 μm. See also Movie S1.

(B and C) Quantification of velocity (B) and arrest coefficient (C) for granuloma-associated p25 and OT-II T cells in BCG- and rBCG30-infected mice. Data points represent individual cells compiled from at least four similar experiments with median values indicated (p < 0.0001 for all OT-II versus p25 comparisons; Mann-Whitney U test).

(D) Liver from a BCG-infected mouse bearing fluorescent populations of p25 and OT-II T cells was fixed, sectioned, and stained with anti-MHC II and a nuclear dye. Scale bar represents 25 μm.

(E) Average instantaneous velocity over time of OT-II (red line) and p25 (green line) granuloma-associated T cells after injection of 25 μg of cognate peptide antigens through an i.v. catheter. Data are representative of three similar experiments. See also Movie S2.

nonspecific populations, there are caveats to the interpretation of these findings. First, the physiological relevance of in vitro stimulated T cells to in vivo primed effectors is unknown and second, the large numbers of transferred T cells may have little relation to the normal numbers of endogenous effectors generated as part of the typical response to infection. Indeed, competition for occupancy of and migration arrest on APCs has been directly demonstrated within lymphoid environments (Garcia et al., 2007). Thus, to establish a more physiologically rele-

T cells (Figure 2D). Therefore, we sequentially injected the peptide antigens for which p25 (Ag85b240) and OT-II (OVA323) T cells are specific, reasoning that rapid loading of surface or re-cycling MHC class II molecules with exogenous peptides would result in strong acute TCR stimulation. Indeed, within 1 min of peptide injection, OT-II and p25 T cells each almost completely arrested their migration in an antigen-specific manner (Figure 2E; Movie S2). Taken together, these data indicate that antigen presentation levels within granulomas are functionally limiting and insufficient to support a high frequency of prolonged effector T cell-APC interactions. These data also establish that migration arrest is a cell-autonomous behavior under these conditions directly linked to specific-antigen recognition.

## Endogenously Primed Antigen-Specific Effector T Cells Show Limited Migrational Arrest in Granulomas

Although adoptive transfer of in vitro generated effector T cells is useful for comparing the dynamics of antigen-specific and

vant system, we crossed the p25 TCR transgenic mice to animals ubiquitously expressing EGFP (Schaefer et al., 2001), maintaining the RAG1 deficiency (p25-EGFP). T cells derived from these mice retain fluorescence even after extensive proliferation and can thus be imaged after transfer into recipient animals as naive cells prior to infection.

Small numbers of antigen-inexperienced p25-EGFP T cells (2000) were transferred into uninfected hosts, which were subsequently infected with BCG, BCGrfp, or rBCG30. This low-dose transfer should yield an EGFP-expressing population in the host animals that is close to a physiological antigen-specific precursor frequency (Hataye et al., 2006). At 2 weeks p.i., EGFP-expressing cells were easily detected in both the liver (Figure 3A; Figure S1; Movie S3) and spleen (Figure S1), indicating a robust antigen-induced expansion in numbers. IM revealed a dynamic population of p25-EGFP T cells, with velocities and arrest coefficients that were similar in BCG- and rBCG30-induced granulomas (Figures 3B and 3C). These findings differ

**Cell PRESS**



**A**

**B**

**C**

**D** Ag85b240
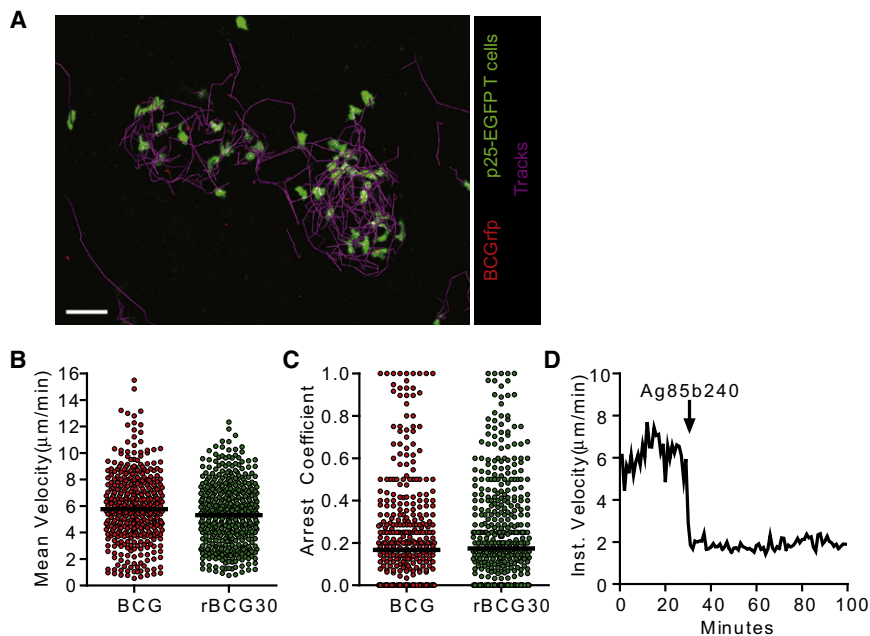
**Figure 3. Limited Evidence of Antigen-Specific Arrest in Mycobacterial Granulomas after In Vivo Priming and Homing of p25-EGFP T Cells**

(A) Representative image from an intravital data set of an animal that had been transferred with p25-EGFP T cells and infected with BCGrfp. The paths of T cell migration through the granuloma over a 30 min time period are shown. Scale bar represents 30 μm. See also Movie S3.

(B and C) Quantification of velocity and arrest coefficient for granuloma-associated p25-EGFP T cells in BCG- and rBCG30-infected mice. Data points represent individual cells compiled from at least four separate experiments with median values indicated (p = 0.0047 in B and p = 0.0475 in C, Mann-Whitney U test).

(D) Instantaneous velocity of the p25-EGFP T cells in a BCG granuloma after administration of Ag85b peptide. See also Figure S1.

from our earlier studies with in vitro stimulated T cells that revealed modest differences in p25 motility in mice infected with the two different strains. The reason for this discrepancy is unknown but could stem from differences in T cell-activation thresholds arising from the different stimulation conditions and/or the fact that, in contrast to acutely transferred effector T cells, the in vivo primed cells represent an asynchronous population that probably arrived in the granuloma over the span of days or weeks as opposed to hours. Nevertheless, injection of Ag85b240 peptide into BCG-infected animals during imaging resulted in rapid and nearly total p25 T cell arrest, indicating that these cells were also capable of responding to robust TCR signals by limiting their migration (Figure 3D). These data again suggest levels of antigen presentation within the granulomas that are insufficient to induce robust TCR signaling in the majority of effector T cells.

## In Vivo Primed Antigen-Specific T Cells Display Limited Effector Cytokine Production

The TCR signaling requirements for induction of T cell effector responses at nonlymphoid sites of tissue inflammation are not well characterized. Although our imaging data suggest that granuloma-associated T cells are not undergoing robust TCR signaling, they could still be receiving adequate stimulation for cytokine production. This might be anticipated based on the widespread upregulation of CD69 reported in Figure 1. Data from previous studies have been interpreted to indicate that T cells can add up sequential weak antigen-induced signals during dynamic movement among a population of APCs and reach a triggering threshold independent of migration arrest on those APCs (Beltman et al., 2007; Celli et al., 2005; Henrickson et al., 2008; Zheng et al., 2008).

To examine the relationship between granuloma-associated T cell motility and effector cytokine production, we examined IFN-γ and TNF-α expression by hepatic p25 T cells after harvest

from the liver. Adoptive transfers of p25-EGFP T cells and infections were performed as in Figure 3, except that 2 hr prior to analysis, animals received an i.v. injection of either PBS or Ag85b240 peptide. Purification of IHLs was performed in the presence of Brefeldin A (BFA) to block protein secretion in situ and allow measurement of cytokine production by hepatic T cells without the need for in vitro restimulation (Reinhardt et al., 2003). Intracellular cytokine staining of IHLs from PBS-treated mice allowed quantification of the frequency of hepatic p25 T cells that were actively producing cytokines at the time of tissue harvest, whereas analysis of IHLs from Ag85b240 peptide-treated animals provided a measure of both the maximal capacity of the hepatic p25 T cell population to produce cytokines after robust stimulation and the cytokine detection limit of the system.

These analyses revealed very low frequencies of hepatic p25 T cells actively producing IFN-γ in BCG-infected animals. Such cells were slightly increased in rBCG30-infected animals, consistent with higher Ag85b expression. Importantly, after i.v. Ag85b240 peptide treatment of BCG-infected mice, the vast majority of p25 T cells showed IFN-γ expression that was markedly increased in amount on a per cell basis relative to PBS-treated animals (Figures 4A–4D), indicating that nearly all these T cells were competent to produce this cytokine. Traditional in vitro PMA+ionomycin (P+I) restimulation revealed a similar increase in cytokine production (Figures 4B–4D), suggesting that in vivo peptide treatment was capable of detecting the full extent of the effector response. Similar results were seen for TNF-α (Figure 4E). These data demonstrate that despite a high capacity for effector cytokine production, IFN-γ and TNF-α expression by hepatic p25 T cells is extremely limited within the granuloma both in terms of the number of cells engaged in such activity and the amount of cytokine being made per cell.

Given that Ag85b240 is a dominant peptide antigen for the T cell response to BCG infection (Huygen et al., 1994), we suspected that a substantial frequency of endogenous T cells would respond to this antigen. Thus, to extend our findings beyond
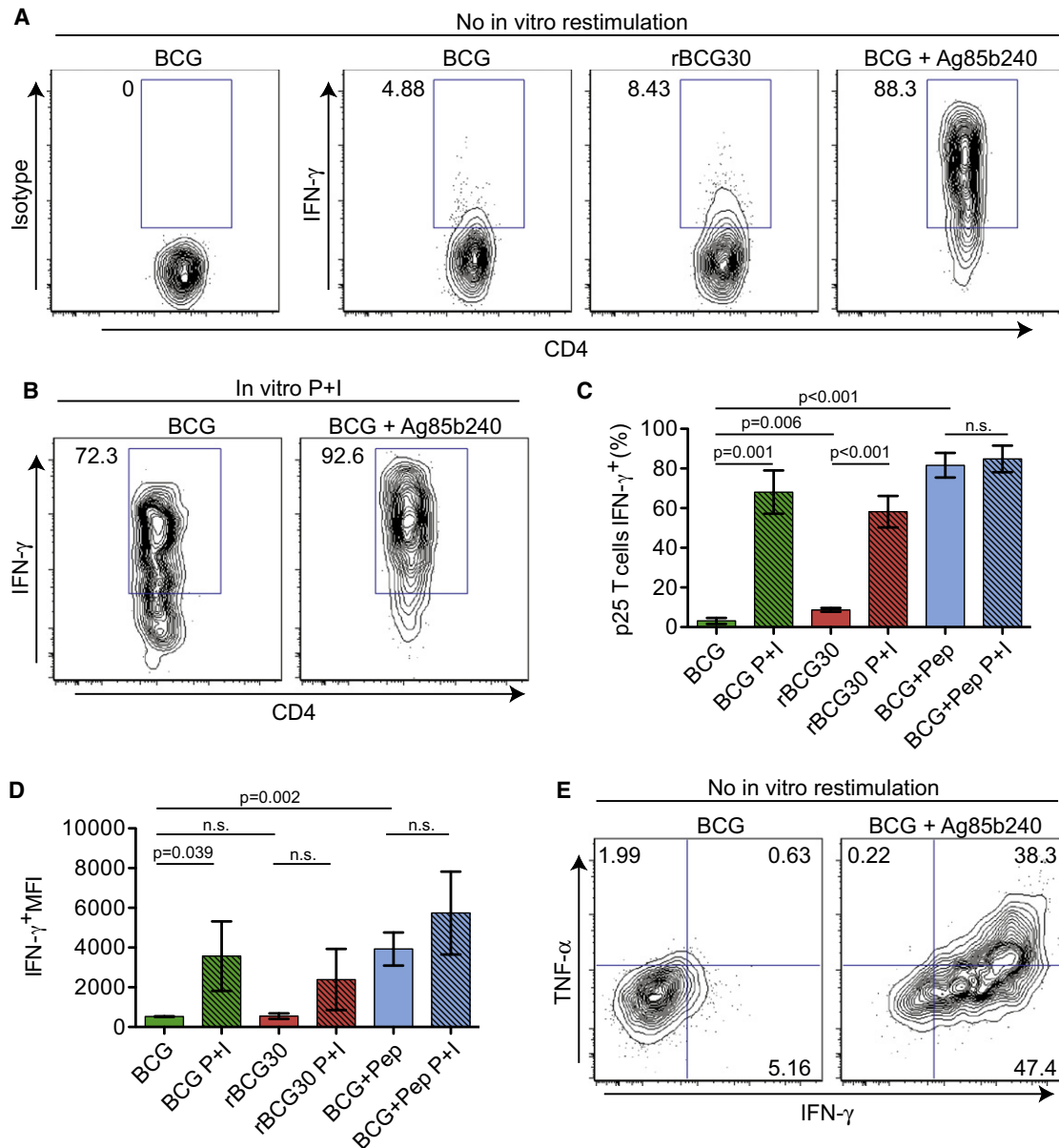
**Figure 4. Antigen-Specific T Cells Show Limited Effector Function but Have High Effector Potential in Mycobacterial Granulomas**

(A and B) Representative histograms gated on CD4$^+$EGFP$^+$ cells from p25-EGFP-bearing, BCG- or rBCG30-infected animals that had been injected with PBS or Ag85b peptide 2 hr prior to analysis or restimulated with P+I in vitro.

(C and D) Quantification of the percentage and MFI of IFN-$\gamma$ p25 T cells. Graphs show mean ± SD from at least three mice per group and are representative of three similar experiments. p values from a two-tailed t test are shown.

(E) Analysis of IFN-$\gamma$ and TNF-$\alpha$ expression by p25-EGFP. See also Figure S2.

TCR transgenic T cells, we also analyzed ex vivo IFN-$\gamma$ expression by endogenous CD4$^+$ T cells with and without i.v. Ag85b240 peptide treatment. Similar to the above findings, only low frequencies of IFN-$\gamma^+$ T cells were observed in the livers of infected mice. Importantly, despite Ag85b240-specific T cells representing only a fraction of the hepatic CD4$^+$ T cell population, we still detected a significant increase in cytokine production after i.v. peptide treatment (Figures S2A and S2B). Thus, although liver-homing T cells are capable of robust Th1 effector cell responses after mycobacterial infection, this capacity for

cytokine expression greatly exceeds what is actively induced by antigen presentation within the granuloma.

The above experiments were focused at 2 week p.i., because this was the earliest point at which we had observed the formation of large numbers of hepatic granulomas and a time of high bacterial burden within the liver (Egen et al., 2008). Preliminary studies performed at 1 week p.i. also revealed low amounts of IFN-$\gamma$ production by endogenous CD4$^+$ T cells (data not shown), suggesting that effector T cells that home to the liver prior to granuloma formation are not engaged in robust cytokine

responses. To exclude the possibility that the maximal granuloma-associated T cell response occurred at later time points, we also examined cytokine responses at 4 weeks p.i., observing an even lower frequency of IFN-$\gamma^+$CD4$^+$ T cells compared to 2 weeks p.i. (Figure S2C). Together with our imaging observations, these data suggest that over the course of granuloma development and maturation, T cell-extrinsic factors, such as limited quantity and/or quality of T cell activation signals, result in highly limited effector T cell responses within granulomas.

## Polarized Secretion of Cytokine by Antigen-Specific, Granuloma-Associated T Cells

In order to relate the small percentage of IFN-$\gamma$-expressing antigen-specific T cells observed by flow cytometry to the spatio-temporal behavior of T cells seen via IM, we examined liver sections from infected animals by immunofluorescence microscopy with antibodies directed against IFN-$\gamma$. Our preliminary studies suggested that this technique had a greatly reduced sensitivity for detection of IFN-$\gamma$ production compared with flow cytometry, and therefore we used rBCG30 infection in order to maximize our chances of detecting small populations of IFN-$\gamma^+$ cells. Adoptive transfers with p25-EGFP T cells were performed as in Figure 3 and livers analyzed 2 weeks p.i. Although no specific staining was observed with an isotype control antibody (Figure 5A), an IFN-$\gamma$-specific antibody showed specific staining within a subset of granuloma-associated p25 T cells, where it appeared in a punctate staining pattern generally polarized to one side of the cell (Figures 5B and 5C). The number of IFN-$\gamma^+$ cells per granuloma was highly variable, with the majority of granulomas containing no detectable staining (not shown). Other granulomas contained small numbers of both p25 and endogenous IFN-$\gamma$ producers (Figure 5B). In a smaller number of cases, large clusters of IFN-$\gamma$-producing p25 T cells could be observed (Figure 5C; Movie S4).

We also compared the localization of mycobacteria and/or mycobacterial antigens within the granuloma to the sites of polarized effector T cell cytokine production by staining for Ag85b protein. We first confirmed that the Ag85b antibody specifically detected BCG within granulomas by staining liver sections derived from BCGrfp-infected mice (Figure S3). The location of BCGrfp and Ag85b were generally overlapping, although there were some instances where Ag85b could be detected in the absence of appreciable BCGrfp fluorescence, perhaps representing locations of bacterial death or sites where antigen has been trafficked away from the bacteria. Although IFN-$\gamma$ staining was generally polarized toward sites of Ag85b localization, because of the large numbers of Ag85b puncta within the granuloma and the extremely high density of macrophages, which limited accurate delineation of individual infected APC, we were unable to generate quantitative correlations between these events. Importantly, however, Ag85b staining was clearly detected at sites distal to both IFN-$\gamma$ production and p25 T cell localization, suggesting that other factors in addition to bacterial localization, such as those affecting antigen processing and presentation within a given APC, may be critical for regulating sites of T cell-antigen recognition and upregulation of effector function. Consistent with this idea, we routinely observed reduced levels of MHC class II within the central region of the granuloma where the majority of mycobacteria are found (Figure S3).

## Limited Frequency of Sustained Antigen-Specific T Cell-APC Interactions within Mtb-Induced Liver Granulomas

To relate the above findings to a more clinically relevant infection, we developed techniques for hepatic IM under biosafety level 3 (BSL-3) conditions, providing the ability to observe granuloma dynamics after infection with virulent Mtb. We first confirmed our ability to image Mtb-induced granulomas by using gene-targeted mice in which EGFP had been placed under the control of the endogenous Lysozyme M promoter (LysM-EGFP). The latter animals were previously used to characterize macrophage dynamics in hepatic BCG-induced granulomas (Egen et al., 2008). IM at 2 weeks p.i. with an i.v. inoculation of 5 × 10$^5$ Mtb revealed well-formed hepatic macrophage aggregates which, consistent with our previously published data, formed a dense network of largely static cells (Figure 6A; Movie S5). Thus, at least in terms of myeloid cell populations, hepatic granuloma dynamics appear similar for BCG and Mtb. These data argue against bacterial virulence determinants that are missing in BCG, such as region of differentiation-1 (RD1), being primary regulators of granuloma-associated macrophage motility in our system, as suggested by previous work with a zebrafish model of mycobacterial infection (Davis and Ramakrishnan, 2009).

Adoptive transfer and imaging of in vitro stimulated, differentially labeled effector OT-II and p25 T cells revealed robust recruitment of both antigen-specific and nonspecific cell populations into Mtb-induced liver granulomas (Figure 6B; Movie S6). However, only small differences were observed in the mean velocity and arrest coefficient between these T cell populations (Figures 6C and 6D). These data are consistent with our findings via BCG infection and suggest that limited antigen presentation within granulomas may be a general feature of mycobacterial infections.

## Limited Effector T Cell Cytokine Secretion within Mtb-Induced Granulomas

We next examined whether the minimal antigen-induced T cell arrest observed in Mtb-induced granulomas would correlate with a paucity of effector cytokine production, as it had after BCG infection. With a similar protocol to that described in Figure 4, we determined both the extent of and capacity for production of IFN-$\gamma$ from p25 effector T cells isolated from Mtb-infected animals in the presence of BFA. Again we detected a low frequency of IFN-$\gamma^+$ p25 T cells directly ex vivo from Mtb-infected animals (Figure 7A). Upon i.v. Ag85b240 peptide injection, the frequency of IFN-$\gamma^+$ cells and the amount of cytokine per cell was dramatically increased (Figures 7A and 7C). Ex vivo restimulation with P+I showed only a modest increase in the frequency of IFN-$\gamma^+$ T cells compared with i.v. peptide administration (Figures 7B and 7C). Thus, the limited arrest of antigen-specific T cells observed in Mtb-induced granulomas appears to translate to muted, submaximal local effector T cell responses within these structures.

## DISCUSSION

Mycobacterial containment relies on the ability of granulomas to spatially and temporally colocalize critical cellular components from the innate and adaptive arms of the immune system to generate antibacterial effector responses. We previously
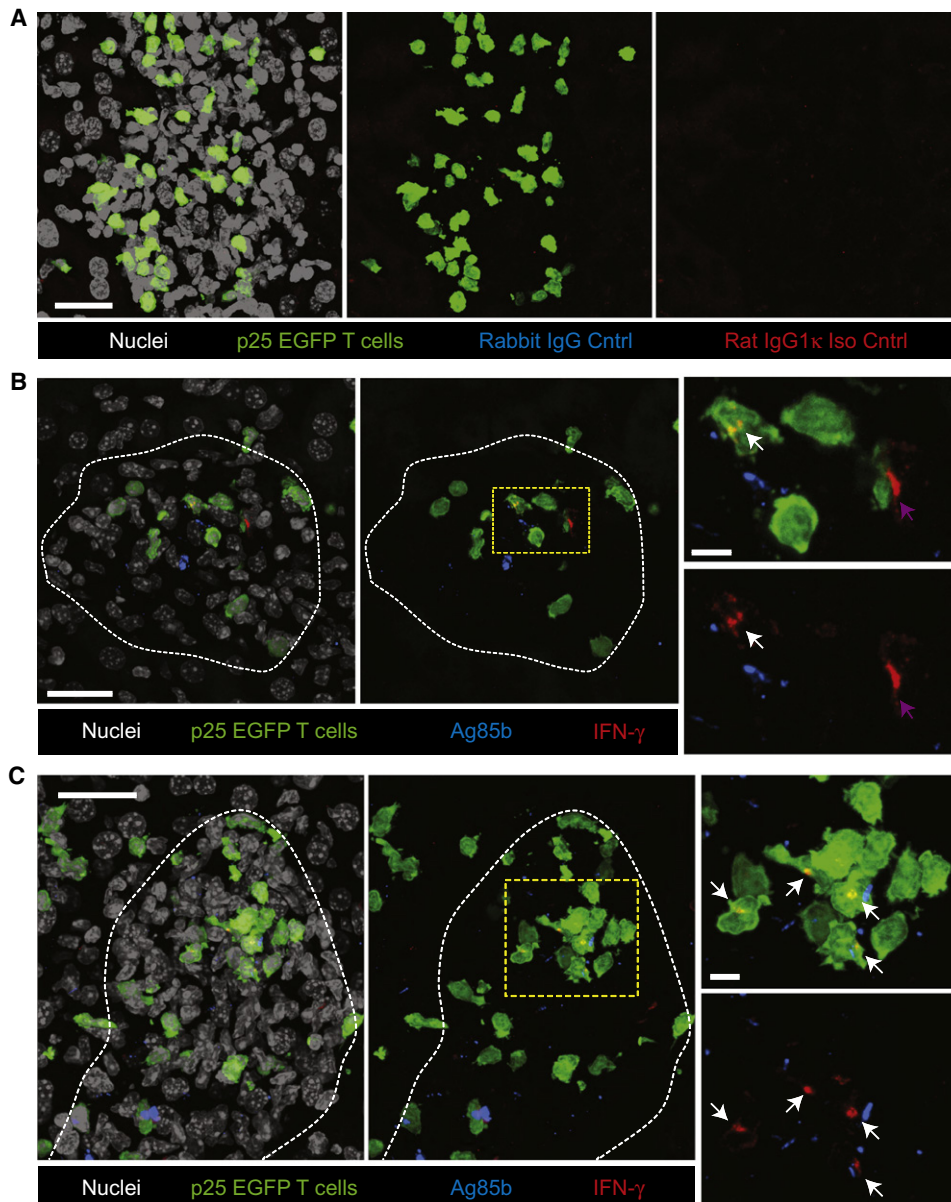
**Figure 5. In Situ IFN-γ Staining in the Livers of rBCG30-Infected Mice**

(A) Control stains for IFN-γ and Ag85b. Livers from rBCG30-infected mice bearing p25-EGFP T cells were fixed, sectioned, and stained with purified rabbit IgG and rat IgG1k as controls for anti-Ag85b and anti-IFN-γ, respectively, and a nuclear counterstain. Images represent a single granuloma and show overlap of all channels (left); overlap of red, green, and blue channels (center); and overlap of red and blue channels (right).

(B and C) Livers from rBCG30-infected mice bearing p25-EGFP T cells were fixed, sectioned, and stained with antibodies specific for Ag85b and IFN-γ and a nuclear counterstain. Two examples of individual granulomas with low (B) and high (C) numbers of IFN-γ⁺ cells are shown. Granuloma borders are delineated with a white line. Images on the right are magnified from boxed region in the central panel and show IFN-γ staining from p25-EGFP T cells (white arrows) and an endogenous T cell (purple arrow). The EGFP signal is removed in the lower panel for clarity.

Scale bars represent 25 μm in large panels and 5 μm in small panels. See also Movie S4.

demonstrated that these lesions in infected mice consist of a largely static macrophage network that supports the rapid recruitment and constrained localization of a highly motile effector T cell population (Egen et al., 2008). Communication between these two cell types is critical for the antimycobacterial response and consists in part of antigen presentation to T cells by infected macrophages and possibly DCs and the subsequent

local activation and production of macrophage-stimulating cytokines by the T cells (Flynn and Chan, 2001).

By using a well-established liver infection model, we demonstrated that few potential effector T cells were stimulated sufficiently by antigen at any one time within a mycobacterial granuloma to elicit inflammatory cytokine production and that this low frequency correlated with the paucity of antigen-specific T cells
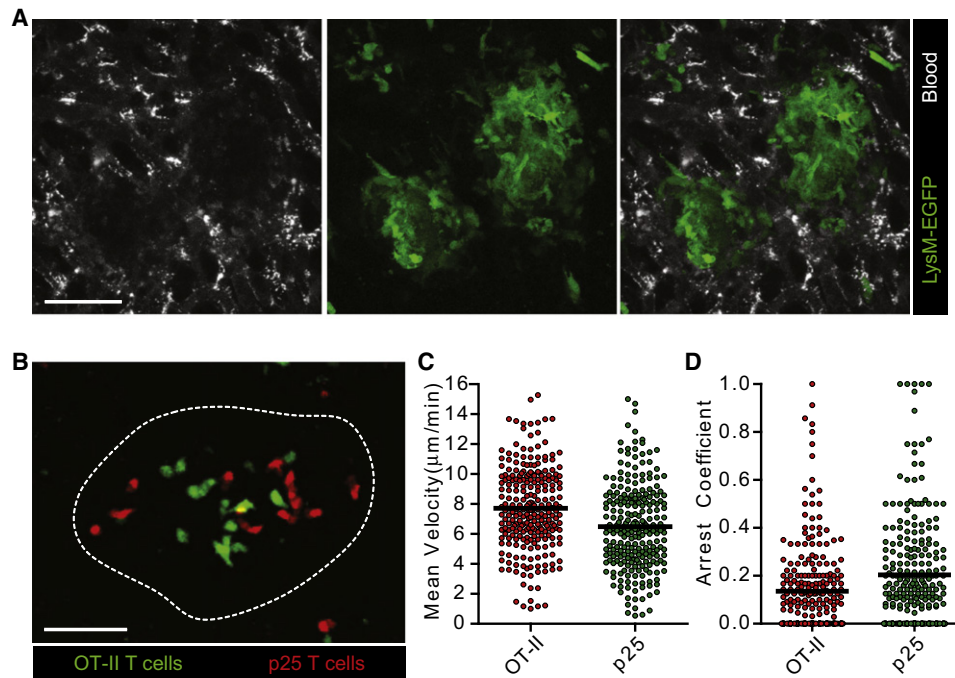
**Figure 6. Intravital Imaging of Mtb-Infected Animals Reveals Limited Antigen Recognition by p25 T Cells**
(A) LysM-EGFP animals were subject to intravital hepatic imaging 2 weeks after i.v. infection with Mtb. See also Movie S5.
(B) CMTPX-labeled p25 and CMFDA-labeled OT-II T cells were transferred i.v. into mice that had been infected with Mtb 2 weeks earlier and imaged 4 hr later. Scale bars represent 50 μm. See also Movie S6.
(C and D) Quantification of velocity and arrest coefficient for granuloma-associated p25 and OT-II T cells in Mtb-infected mice. Data points represent individual cells compiled from at least four separate experiments with median values indicated (p < 0.0001 in C and p = 0.0003 in D, Mann-Whitney U test).

showing migration arrest under several conditions. Yet nearly all the T cells were capable of showing migration arrest and responding with a much higher amount of per cell cytokine production if confronted with artificially raised amounts of antigen. From these data we conclude that, despite being sufficient for constraining the infection, the display of antigenic complexes by the myeloid compartment within a granuloma is functionally limited, such that at any moment, only a small number of T cells can be triggered to arrest migration and produce relatively modest levels of cytokines.

We speculate that these data via a hepatic infection model are highly relevant to and predictive of events that occur during more physiologically relevant pulmonary infections with Mtb. Indeed, systemic infection models have been used extensively to examine the cellular and molecular pathways involved in host responses to Mtb. However, similar experiments in low-dose aerosol Mtb infection models will be an important step in determining the extent to which our findings relate to the pathogenesis of human tuberculosis. In addition, our studies primarily examined the effector response to a single mycobacterial antigen via a TCR transgenic adoptive transfer model. Although we demonstrate that the bulk population of endogenous CD4^{+} T cells behaves similarly to our transferred population in terms of producing a muted, submaximal effector cytokine response, future work aimed at examining T cell recognition of additional mycobacterial antigens is needed to determine the extent to which our findings can be generalized.

Although often speculated upon, the correlation between T cell motility and effector cytokine production has not been

well established. Our analysis of local cytokine production within the liver without additional in vitro restimulation revealed that, despite highly efficient Th1 cell polarization during priming and recruitment of mycobacterial antigen-specific effector T cells into granulomas, only small numbers of these cells actively produce IFN-γ and/or TNF-α at any one time. Thus, cytokine production appears linked with motility and similar TCR signaling thresholds may be in place for regulating both migration arrest and upregulation of effector function. The rare T cells that do receive sufficient signals to cause arrest synthesize cytokine that, at least in the case of IFN-γ, is secreted in a spatially polarized fashion, presumably resulting in highly localized delivery of the effector protein to limited numbers of target APCs. These data are consistent with previous findings demonstrating polarized secretion of IFN-γ by CD8^{+} T cells toward virally infected targets in the brain (Barcia et al., 2008). Interestingly, we also observed rare cases of clustered cytokine-producing T cells, suggesting the existence of extremely localized regions of more robust antigen presentation within some granulomas. These data are reminiscent of previous findings showing heterogeneity and local variation in T cell responses to *Leishmania major*-infected cells in the skin (Filipe-Santos et al., 2009).

Numerous studies have identified mycobacterial pathways capable of limiting antigen presentation by infected cells, especially via the MHC class II pathway (Harding and Boom, 2010). In addition, downregulation of costimulatory molecules from the surface of APCs and upregulation of inhibitory receptors capable of locally suppressing the T cell response could also result in
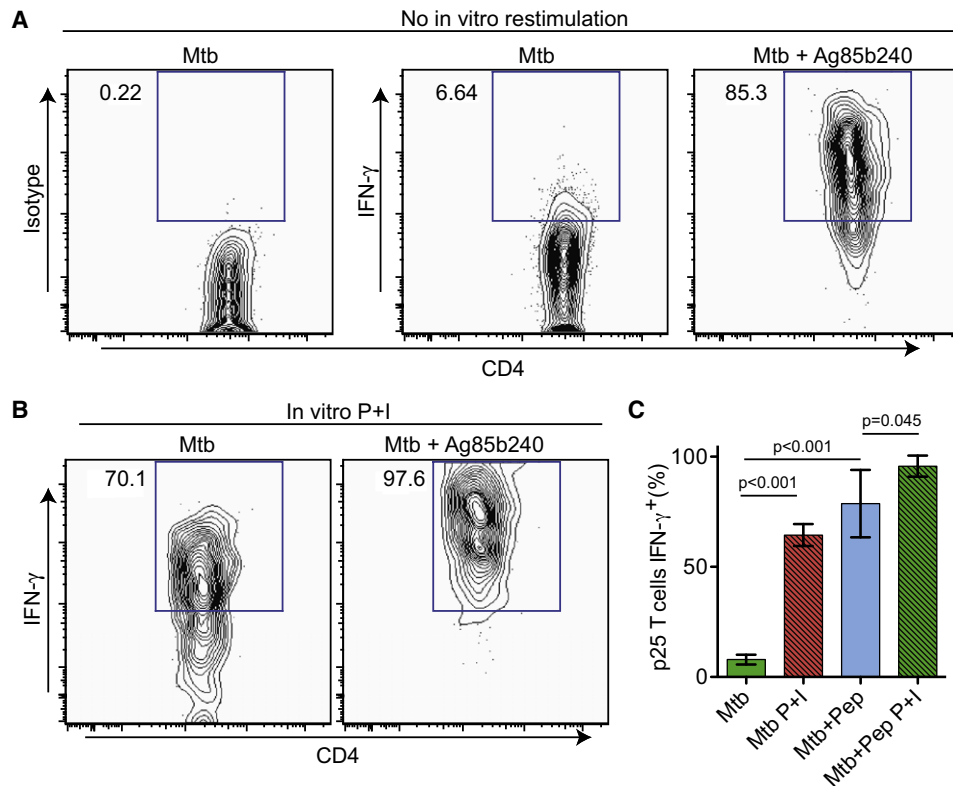
**Figure 7. Antigen-Specific T Cells Show Limited Effector Function but High Effector Potential in Mtb-Induced Granulomas**
(A) Animals were treated as in Figure 4 except they were infected with Mtb. Representative histograms gated on CD4$^+$EGFP$^+$ cells from p25-EGFP-bearing infected animals that had been injected with PBS or Ag85b peptide 2 hr prior to analysis.
(B) IHLs were restimulated with P+I prior to analysis in order to detect maximum cytokine production.
(C) Quantification of percentage of p25 T cells expressing IFN-γ. Graph shows mean ± SD from at least three mice per group and is representative of two similar experiments. p values from a two-tailed t test are shown.

limited effector function within the granuloma (Schreiber et al., 2010). It is likely that these immune evasion mechanisms are at least partly responsible for the low effector CD4$^+$ T cell arrest and cytokine production observed in this study. However, other factors may also influence the frequency of arrested and cytokine-producing T cells detected in granulomas. During the initial response to suboptimal TCR stimuli in the LN, naive T cells are thought to integrate signals derived from multiple encounters with APCs until a threshold is reached for arrest (Henrickson et al., 2008; Mempel et al., 2004). We did observe a high frequency of T cells showing signs of activation shortly after homing to the infected liver but were unable to determine whether those T cells receiving low levels of stimulatory signals became more prone to arrest at later time points. Examination of in vitro generated effector T cell motility 12–24 hr posttransfer did not reveal greater frequencies of arrested T cells compared to early time points (not shown), but these experiments are difficult to interpret because we were unable to prevent continual T cell homing into the granuloma, thus leading to a temporally asynchronous population at later time points. An additional possibility is that rare T cells encountering high amounts of cognate antigen could eventually desensitize TCR signaling pathways leading to an increased threshold for arrest. Consistent with this idea, in vivo primed p25-EGFP T cells that had homed to the granuloma over the course of

days to weeks did not show the difference in motility between BCG- and rBCG30-infected animals that was apparent in experiments with acutely transferred effector T cells examined within 4 hr of their entry into these structures. Thus, an interesting possibility is that effector T cells at sites of chronic inflammation can adjust their stimulation threshold in order to strike a balance between protection and immune-mediated tissue destruction.

Recently, several publications have concluded that effector T cell arrest is rare at sites of chronic infection (Beattie et al., 2010; Filipe-Santos et al., 2009; Schaeffer et al., 2009; Wilson et al., 2009). Although these studies did not examine the relationship between motility and cytokine production, together with our study they suggest that limited long-term T cell-APC interactions and correspondingly low levels of effector responses may be a general feature of persistent infections and emphasize the importance of determining whether bulk population behavior or the dynamic properties of only a minor fraction of imaged cells is the relevant parameter for measurement in such cases. Comparing these data to future studies aimed at examining effector T cell motility and effector cytokine production in acutely resolving infection models should be informative, because we speculate that rapidly resolving infections may induce more robust effector T cell responses capable of effectively clearing the invading pathogen.

The data presented here reveal that, relative to their potential, effector T cells migrating within mycobacterial granulomas produce an extremely muted response as a result of limited local antigen presentation and/or recognition. An implication of these findings is that strategies aimed solely at expanding the pool of antigen-specific effector T cells in individuals infected with some persistent pathogens, such as Mtb, may meet with limited success, because there may be insufficient antigen present at sites of infection to support additional effector responses. Rather, immunotherapeutic approaches designed to both increase levels of local antigen presentation and maintain a high frequency of effector T cells within infected tissues will probably have the best chance at successfully reversing the course of the disease.

## EXPERIMENTAL PROCEDURES

### Mice

C57BL/6 OT-II TCR transgenic RAG1-deficient mice were from Taconic Laboratories. C57BL/6 p25 TCR transgenic RAG1-deficient animals were kindly provided by J. Ernst (New York University School of Medicine, New York) (Wolf et al., 2008). C57BL/6 LysM-EGFP knockin animals were provided by T. Graf (Center for Genomic Regulation, Barcelona, Spain) (Faust et al., 2000). C57BL/6 mice and transgenic mice expressing EGFP under the control of the human ubiquitin C promoter (Schaefer et al., 2001) were from Jackson Laboratories. All mice were maintained in specific-pathogen-free conditions at an Association for Assessment and Accreditation of Laboratory Animal Care-accredited animal facility at the NIAID. All procedures were approved by the NIAID Animal Care and Use Committee (National Institutes of Health, Bethesda, MD).

### Mycobacterial Strains and Infection

*Mycobacterium tuberculosis* strain H37Rv, *Mycobacterium bovis* BCG strain Pasteur, RFP-expressing BCG strain Pasteur (Abadie et al., 2005), and rBCG30 Tice overexpressing Ag85b (Horwitz et al., 2000) were expanded to log phase on Middlebrook 7H9 liquid medium supplemented with ADC (Difco), washed, aliquoted in PBS, and stored at $-80^\circ$C until further use. BCG-RFP and rBCG30 bacteria were grown in the presence of Hygromycin (Sigma). Bacterial stocks were quantified on 7H11 agar supplemented with OADC (Difco). For mycobacterial infections, animals were inoculated i.v. with $3 \times 10^6$ BCG or $5 \times 10^5$ Mtb in PBS.

### In Vitro T Cell Stimulation and Adoptive Transfers

For in vitro generated effector T cells, LNs were disrupted by passing through a 70 $\mu$m cell strainer (BD Biosciences). $1 \times 10^6$ of the isolated cells were stimulated with $1 \times 10^7$ mitomycin C-treated C57BL/6 splenocytes in complete RPMI 1640 (10% FCS, 2 mM L-glutamine, 50 $\mu$M 2-mercaptoethanol, and penicillin/streptomycin) plus 2 $\mu$M ovalbumin 323-339 peptide (OT-II) or Ag85b 240-254 peptide (p25) in each well of a 24-well plate. Two days after stimulation, cells were expanded in the presence of 30 U/ml recombinant human IL-2 (R&D systems) and used for experiments 6–7 days postactivation. In vitro generated effector T cells were labeled with 1 $\mu$M CMTPX or CMFDA (Invitrogen) for 15 min at 37$^\circ$C in HBSS. $1 \times 10^7$ of each cell type was injected i.v. into recipient animals.

For antigen-inexperienced T cells, LN cells obtained from p25-EGFP mice (>90% V$\beta$11$^+$CD4$^+$ T cells) were transferred into noninfected recipient animals. Each animal received $2 \times 10^3$ p25 T cells. Animals were infected ~12 hr later as described above.

### Cell Isolation and Flow Cytometry

For intrahepatic lymphocyte isolation, livers were perfused through the portal vein with RPMI+1% fetal calf serum containing 0.25 mg/ml of Liberase CI (Roche) and 0.05% DNase I (Boehringer Mannheim), excised, and digested for an additional 45 min at 37$^\circ$C. Cell suspensions were washed, resuspended in a 33% isotonic Percoll (Amersham Biosciences), and centrifuged at 800 $\times$ g for 20 min.

For analysis of adoptively transferred, in vitro stimulated effector T cells, IHLs were stained with anti-CD4 Pacific Blue (Clone RM4-5), anti-CD3 Alexa

Fluor (AF) 647 (Clone 17A2). Anti-CD69 PE-Cy7 (Clone H1.2F3) was used in some experiments. CMFDA- and CMTPX-labeled cells were detected in the FITC and PE-Texas Red channels, respectively. For analysis of intracellular cytokine production, cell suspensions were obtained as described above except that 20 $\mu$g/ml of BFA (Sigma) was included in the digest buffer and subsequent steps were performed in the presence of 5 $\mu$g/ml BFA. Cells were stained immediately ex vivo or stimulated in vitro for 2 hr at 37$^\circ$C in the presence of 20 ng/ml phorbol 12-myristate 13-acetate, 1 $\mu$M ionomycin, and 10 $\mu$g/ml of BFA (All from Sigma). Cells were surface stained with anti-CD4 Pacific Blue, anti-V$\beta$11 biotin (Clone RR3-15), and anti-CD3 PerCP-Cy5.5 (Clone 145-2C11). Biotinylated antibodies were detected with Streptavidin PE-Cy7. Cells were fixed with Cytofix buffer, permeabilized with Perm/Wash buffer (BD Biosciences), and stained with anti-IFN-$\gamma$ AF647 (Clone XMG1.2) and anti-TNF-$\alpha$ PE (Clone MP6-XT22). EGFP was detected in the FITC channel and isotype controls were used to determine background signals for intracellular stains. Flow cytometric data were collected on an LSR II (BD Biosciences) and analyzed with FlowJo software (TreeStar).

### Intravital Multiphoton Microscopy

Surgical preparation of the liver was performed as described (Egen et al., 2008). Liver sinusoids were visualized by injecting Texas Red-conjugated bovine serum albumin (BSA-TR), AF647-conjugated BSA (BSA-647), or non-targeted Quantum Dots 705 (Invitrogen) i.v. immediately prior to imaging. For acute injection of peptide antigens during imaging, a catheter was placed into the tail vein via a 30GA needle attached to PE-10 tubing (Becton Dickinson) and secured with Durapore Tape (Fischer Scientific). For BCG-infected animals, images were acquired on an LSM 510 NLO multiphoton imaging system (Carl Zeiss Microimaging) as described in (Egen et al., 2008). For Mtb-infected animals, images were acquired on a TCS-SP2 MP inverted confocal microscope (Leica Microsystems) located in a dedicated BSL-3 suite, with a 20$\times$/0.7 NA objective for imaging. Fluorescence excitation was provided by a Chameleon Ti:Sapphire laser (Coherent). EGFP and RFP were excited at 920 nm while CMFDA and CMTPX were excited at 820 nm. For 4-dimensional (4D) data sets, 3-dimensional stacks were captured every 1 min, unless otherwise specified.

Raw imaging data were processed with Imaris (Biplane). Automatic object tracking via Imaris Spots was aided with manual corrections to retrieve cell spatial coordinates over time that were analyzed in MatLab. Arrest coefficient was defined as the percentage of time points a cell's instantaneous velocity was less than 2 $\mu$m/min. AfterEffects (Adobe) was used to produce video clips.

### Immunofluorescence Staining

Livers were perfused with PBS followed by PLP buffer (0.05 M phosphate buffer containing 0.1 M L-lysine [pH 7.4], 2 mg/ml NaIO$_4$, and 10 mg/ml para-formaldehyde), fixed for an additional 12 hr, and dehydrated in 30% sucrose prior to embedding in OCT freezing media (Sakura Finetek). 16 $\mu$m sections were cut on a CM3050S cryostat (Leica) and adhered to Superfrost Plus slides (VWR). Sections were permeabilized and blocked in PBS containing 0.1% Triton X-100 (Sigma) and 10% goat serum (Jackson Immunoresearch) followed by staining in PBS containing 0.01% Triton X-100 and 5% goat serum. The following antibodies were used: anti-MHC-II FITC (clone 2G9), anti-IFN-$\gamma$ AF647 (Clone XMG1.2; BD Biosciences), anti-F4/80 AF647 (clone BM8; Ebioscience), and anti-Ag85b (AbCam). Unconjugated primary antibodies were stained with AF-conjugated secondary antibodies (Invitrogen). For IFN-$\gamma$ detection, staining with a secondary goat anti-rat AF647 was used to increase the signal. Nuclei were detected with Hoechst 33342 (Invitrogen). Stained slides were mounted with Prolong Gold (Invitrogen) and images were acquired on a LSM 510 or 710 confocal microscope (Carl Zeiss Microimaging).

## SUPPLEMENTAL INFORMATION

Supplemental Information includes three figures and six movies and can be found with this article online at doi:10.1016/j.immuni.2011.03.022.

## ACKNOWLEDGMENTS

## REFERENCES

Abadie, V., Badell, E., Douillard, P., Ensergueix, D., Leenen, P.J., Tanguy, M., Fiette, L., Saeland, S., Gicquel, B., and Winter, N. (2005). Neutrophils rapidly migrate via lymphatics after *Mycobacterium bovis* BCG intradermal vaccination and shuttle live bacilli to the draining lymph nodes. Blood *106*, 1843–1850.

Barcia, C., Wawrowsky, K., Barrett, R.J., Liu, C., Castro, M.G., and Lowenstein, P.R. (2008). In vivo polarization of IFN-gamma at Kupfer and non-Kupfer immunological synapses during the clearance of virally infected brain cells. J. Immunol. *180*, 1344–1352.

Barnden, M.J., Allison, J., Heath, W.R., and Carbone, F.R. (1998). Defective TCR expression in transgenic mice constructed using cDNA-based alpha- and beta-chain genes under the control of heterologous regulatory elements. Immunol. Cell Biol. *76*, 34–40.

Bartholomäus, I., Kawakami, N., Odoardi, F., Schläger, C., Miljkovic, D., Ellwart, J.W., Klinkert, W.E., Flügel-Koch, C., Issekutz, T.B., Wekerle, H., and Flügel, A. (2009). Effector T cell interactions with meningeal vascular structures in nascent autoimmune CNS lesions. Nature *462*, 94–98.

Beattie, L., Peltan, A., Maroof, A., Kirby, A., Brown, N., Coles, M., Smith, D.F., and Kaye, P.M. (2010). Dynamic imaging of experimental *Leishmania donovani*-induced hepatic granulomas detects Kupffer cell-restricted antigen presentation to antigen-specific CD8 T cells. PLoS Pathog. *6*, e1000805.

Beltman, J.B., Marée, A.F., and de Boer, R.J. (2007). Spatial modelling of brief and long interactions between T cells and dendritic cells. Immunol. Cell Biol. *85*, 306–314.

Bousso, P. (2008). T-cell activation by dendritic cells in the lymph node: Lessons from the movies. Nat. Rev. Immunol. *8*, 675–684.

Bousso, P., and Robey, E. (2003). Dynamics of CD8+ T cell priming by dendritic cells in intact lymph nodes. Nat. Immunol. *4*, 579–585.

Caruso, A.M., Serbina, N., Klein, E., Triebold, K., Bloom, B.R., and Flynn, J.L. (1999). Mice deficient in CD4 T cells have only transiently diminished levels of IFN-gamma, yet succumb to tuberculosis. J. Immunol. *162*, 5407–5416.

Celli, S., Garcia, Z., and Bousso, P. (2005). CD4 T cells integrate signals delivered during successive DC encounters in vivo. J. Exp. Med. *202*, 1271–1278.

Davis, J.M., and Ramakrishnan, L. (2009). The role of the granuloma in expansion and dissemination of early tuberculous infection. Cell *136*, 37–49.

Egen, J.G., Rothfuchs, A.G., Feng, C.G., Winter, N., Sher, A., and Germain, R.N. (2008). Macrophage and T cell dynamics during the development and disintegration of mycobacterial granulomas. Immunity *28*, 271–284.

Faust, N., Varas, F., Kelly, L.M., Heck, S., and Graf, T. (2000). Insertion of enhanced green fluorescent protein into the lysozyme gene creates mice with green fluorescent granulocytes and macrophages. Blood *96*, 719–726.

Fife, B.T., Pauken, K.E., Eagar, T.N., Obu, T., Wu, J., Tang, Q., Azuma, M., Krummel, M.F., and Bluestone, J.A. (2009). Interactions between PD-1 and PD-L1 promote tolerance by blocking the TCR-induced stop signal. Nat. Immunol. *10*, 1185–1192.

Filipe-Santos, O., Pescher, P., Breart, B., Lippuner, C., Aebischer, T., Glaichenhaus, N., Späth, G.F., and Bousso, P. (2009). A dynamic map of antigen recognition by CD4 T cells at the site of Leishmania major infection. Cell Host Microbe *6*, 23–33.

Flynn, J.L., and Chan, J. (2001). Immunology of tuberculosis. Annu. Rev. Immunol. *19*, 93–129.

Garcia, Z., Pradelli, E., Celli, S., Beuneu, H., Simon, A., and Bousso, P. (2007). Competition for antigen determines the stability of T cell-dendritic cell interactions during clonal expansion. Proc. Natl. Acad. Sci. USA *104*, 4553–4558.

Harding, C.V., and Boom, W.H. (2010). Regulation of antigen presentation by *Mycobacterium tuberculosis*: A role for Toll-like receptors. Nat. Rev. Microbiol. *8*, 296–307.

Hataye, J., Moon, J.J., Khoruts, A., Reilly, C., and Jenkins, M.K. (2006). Naive and memory CD4+ T cell survival controlled by clonal abundance. Science *312*, 114–116.

Henrickson, S.E., Mempel, T.R., Mazo, I.B., Liu, B., Artyomov, M.N., Zheng, H., Peixoto, A., Flynn, M.P., Senman, B., Junt, T., et al. (2008). T cell sensing of antigen dose governs interactive behavior with dendritic cells and sets a threshold for T cell activation. Nat. Immunol. *9*, 282–291.

Horwitz, M.A., Harth, G., Dillon, B.J., and Maslesa-Galic', S. (2000). Recombinant bacillus calmette-guerin (BCG) vaccines expressing the *Mycobacterium tuberculosis* 30-kDa major secretory protein induce greater protective immunity against tuberculosis than conventional BCG vaccines in a highly susceptible animal model. Proc. Natl. Acad. Sci. USA *97*, 13853–13858.

Huygen, K., Lozes, E., Gilles, B., Drowart, A., Palfliet, K., Jurion, F., Roland, I., Art, M., Dufaux, M., Nyabenda, J., et al. (1994). Mapping of TH1 helper T-cell epitopes on major secreted mycobacterial antigen 85A in mice infected with live *Mycobacterium bovis* BCG. Infect. Immun. *62*, 363–370.

Kawakami, N., Nägerl, U.V., Odoardi, F., Bonhoeffer, T., Wekerle, H., and Flügel, A. (2005). Live imaging of effector cell trafficking and autoantigen recognition within the unfolding autoimmune encephalomyelitis lesion. J. Exp. Med. *201*, 1805–1814.

Kim, J.V., Kang, S.S., Dustin, M.L., and McGavern, D.B. (2009). Myelomonocytic cell recruitment causes fatal CNS vascular injury during acute viral meningitis. Nature *457*, 191–195.

Ladel, C.H., Daugelat, S., and Kaufmann, S.H. (1995). Immune response to *Mycobacterium bovis* bacille Calmette Guérin infection in major histocompatibility complex class I- and II-deficient knock-out mice: contribution of CD4 and CD8 T cells to acquired resistance. Eur. J. Immunol. *25*, 377–384.

Matheu, M.P., Beeton, C., Garcia, A., Chi, V., Rangaraju, S., Safrina, O., Monaghan, K., Uemura, M.I., Li, D., Pal, S., et al. (2008). Imaging of effector memory T cells during a delayed-type hypersensitivity reaction and suppression by Kv1.3 channel block. Immunity *29*, 602–614.

Mempel, T.R., Henrickson, S.E., and Von Andrian, U.H. (2004). T-cell priming by dendritic cells in lymph nodes occurs in three distinct phases. Nature *427*, 154–159.

Miller, M.J., Wei, S.H., Parker, I., and Cahalan, M.D. (2002). Two-photon imaging of lymphocyte motility and antigen response in intact lymph node. Science *296*, 1869–1873.

Miller, M.J., Safrina, O., Parker, I., and Cahalan, M.D. (2004). Imaging the single cell dynamics of CD4+ T cell activation by dendritic cells in lymph nodes. J. Exp. Med. *200*, 847–856.

Mogues, T., Goodrich, M.E., Ryan, L., LaCourse, R., and North, R.J. (2001). The relative importance of T cell subsets in immunity and immunopathology of airborne *Mycobacterium tuberculosis* infection in mice. J. Exp. Med. *193*, 271–280.

Reinhardt, R.L., Bullard, D.C., Weaver, C.T., and Jenkins, M.K. (2003). Preferential accumulation of antigen-specific effector CD4 T cells at an antigen injection site involves CD62E-dependent migration but not local proliferation. J. Exp. Med. *197*, 751–762.

Sancho, D., Gómez, M., and Sánchez-Madrid, F. (2005). CD69 is an immunoregulatory molecule induced following activation. Trends Immunol. *26*, 136–140.

Saunders, B.M., and Britton, W.J. (2007). Life and death in the granuloma: Immunopathology of tuberculosis. Immunol. Cell Biol. *85*, 103–111.

Schaefer, B.C., Schaefer, M.L., Kappler, J.W., Marrack, P., and Kedl, R.M. (2001). Observation of antigen-dependent CD8+ T-cell/dendritic cell interactions in vivo. Cell. Immunol. *214*, 110–122.

Schaeffer, M., Han, S.J., Chtanova, T., van Dooren, G.G., Herzmark, P., Chen, Y., Roysam, B., Striepen, B., and Robey, E.A. (2009). Dynamic imaging of T cell-parasite interactions in the brains of mice chronically infected with *Toxoplasma gondii*. J. Immunol. *182*, 6379–6393.

Schreiber, H.A., Hulseberg, P.D., Lee, J., Prechl, J., Barta, P., Szlavik, N., Harding, J.S., Fabry, Z., and Sandor, M. (2010). Dendritic cells in chronic mycobacterial granulomas restrict local anti-bacterial T cell response in a murine model. PLoS ONE *5*, e11453.

Skokos, D., Shakhar, G., Varma, R., Waite, J.C., Cameron, T.O., Lindquist, R.L., Schwickert, T., Nussenzweig, M.C., and Dustin, M.L. (2007). Peptide-MHC potency governs dynamic interactions between T cells and dendritic cells in lymph nodes. Nat. Immunol. *8*, 835–844.

Stoll, S., Delon, J., Brotz, T.M., and Germain, R.N. (2002). Dynamic imaging of T cell-dendritic cell interactions in lymph nodes. Science *296*, 1873–1876.

Tamura, T., Ariga, H., Kinashi, T., Uehara, S., Kikuchi, T., Nakada, M., Tokunaga, T., Xu, W., Kariyone, A., Saito, T., et al. (2004). The role of antigenic peptide in CD4$^+$ T helper phenotype development in a T cell receptor transgenic model. Int. Immunol. *16*, 1691–1699.

Ulrichs, T., and Kaufmann, S.H. (2006). New insights into the function of granulomas in human tuberculosis. J. Pathol. *208*, 261–269.

Wilson, E.H., Harris, T.H., Mrass, P., John, B., Tait, E.D., Wu, G.F., Pepper, M., Wherry, E.J., Dzierzinski, F., Roos, D., et al. (2009). Behavior of parasite-specific effector CD8$^+$ T cells in the brain and visualization of a kinesis-associated system of reticular fibers. Immunity *30*, 300–311.

Wolf, A.J., Desvignes, L., Linas, B., Banaiee, N., Tamura, T., Takatsu, K., and Ernst, J.D. (2008). Initiation of the adaptive immune response to *Mycobacterium tuberculosis* depends on antigen production in the local lymph node, not the lungs. J. Exp. Med. *205*, 105–115.

Zheng, H., Jin, B., Henrickson, S.E., Perelson, A.S., von Andrian, U.H., and Chakraborty, A.K. (2008). How antigen quantity and quality determine T-cell decisions in lymphoid tissue. Mol. Cell. Biol. *28*, 4040–4051.